

# The Central Neutron Detector

P. Chatagnon<sup>a</sup>, J. Bettane<sup>a</sup>, G. Hull<sup>a</sup>, M. Imre<sup>a</sup>, D. Marchand<sup>a</sup>, B. Mathon<sup>a</sup>, G. Murdoch<sup>b</sup>, P. Naidoo<sup>b</sup>, S. Niccolai<sup>a</sup>, K. Price<sup>a</sup>, D. Sokhan<sup>b</sup>, R. Wang<sup>a</sup>

<sup>a</sup>*Institut de Physique Nucléaire, CNRS-IN2P3, Univ. Paris-Sud, Université Paris-Saclay, 91406 Orsay Cedex, France*

<sup>b</sup>*University of Glasgow, Glasgow G12 8QQ, United Kingdom*

---

## Abstract

The Central Neutron Detector is a scintillator barrel that was designed to detect 0.2-1 GeV neutrons at backwards angles in the CLAS12 spectrometer in Hall B at Jefferson Laboratory. The design is based on three radial layers of paddles readout at the upstream end of the barrel by photomultiplier tubes. Neighboring paddles in each layer are coupled together at the downstream end of the barrel by “U-turn” lightguides. The components of this detector are presented and performance of the detector with the first beam data taken by CLAS12 is reported.

---

## 1. Overview

The Central Neutron Detector (CND) is the outermost of the subsystems composing the Central Detector of CLAS12. It consists of a barrel of three layers of scintillators coupled at their downstream ends with U-turn light guides and read out at their upstream ends by photomultiplier tubes (PMTs) connected to the bars via 1-m-long bent light guides to position them in a fringe-field region of the CLAS12 5-T superconduction solenoid. The CND was installed in the CLAS12 solenoid, and subsequently started its data taking, in the fall of 2017. GEANT4-based simulations, calibrated with measurements carried out with the CND using cosmic rays muons, showed that the efficiencies obtainable with this detector and its photon-rejection capabilities are sufficient to collect good statistics on the beam-spin asymmetry for the neutron-DVCS reaction over a wide phase space, using the allocated beam time for CLAS12 with a deuterium target [1]. The first beam data collected by CLAS12 on a proton target confirmed the design performances. This detector will also be used in other  $n$ -DVCS experiments [2], and whenever the detection of the recoil neutron may be required ( $N^*$  program, for instance, or all the deeply-virtual meson production reactions on the neutron).

## 2. Requirements

Measuring Deeply Virtual Compton Scattering (DVCS) on a neutron target ( $en \rightarrow e'n'\gamma$ ) is one of the necessary steps to complete our understanding of the

structure of the nucleon in terms of Generalized Parton Distributions (GPDs) [3, 4, 5]. DVCS on a neutron target allows one to perform a quark-flavor decomposition of the GPDs, combined with the results for DVCS on a proton target. Moreover, it plays a complementary role to DVCS on a transversely polarized proton target in the determination of the GPD  $E$ , the least known and least constrained GPD that enters Ji’s sum rule [4], which links integrals of GPDs to the total angular momentum of the quarks. To measure  $n$ -DVCS on a deuterium target ( $ed \rightarrow e'n\gamma(p)$ ) with CLAS12, the electron and the DVCS photon, emitted mainly at small angles, can be detected in the CLAS12 forward calorimeters (ECAL [6] and FT[7]), while the neutron is emitted predominantly (for  $\sim 80\%$  of the events) at  $\theta > 40^\circ$  in the laboratory frame, with an average momentum around 0.5 GeV. These kinematic constraint conditions drive the design specifications for the CND. With the aid of the CLAS12 fast Monte Carlo tool (FASTMC), the requirements in terms of angular and momentum resolutions on the detected neutrons were determined by studying the missing mass (“ $MM$ ”) of the  $e'n'\gamma$  system. Using realistic resolutions on the electron and photon calculated by FASTMC, it was found that if the neutron momentum resolution is kept below 10% its effect on the  $MM$  resolution is negligible with respect to the other particles in the reaction [8].

Therefore, considering that the detection capabilities of CLAS12 for electrons and high-energy photons are fixed, the requirements of the CND are:

- good neutron identification capabilities for the

kinematic range of interest ( $0.2 < p_n < 1.2$  GeV,  
 $40^\circ < \theta_n < 80^\circ$ );

- neutron momentum resolution  $\sigma_P/P$  within 10%.

### 2.1. Constraints

The available space in the CLAS12 Cetral Detector is limited by the presence of the CTOF and of the solenoid magnet, which left about 10 cm free. However, the CTOF can also be used to detect neutrons, adding an additional 2-3% of detection efficiency. The central tracker can be used as a veto for charged particles. Finally, the strong fringe field of the 5-T magnetic field required careful consideration for the positioning and the type of the CND PMTs.

After extensive GEANT4 simulations and R&D studies devoted to examine the various options for the CND and its possible photodetectors [8], the final design choice was a barrel of standard plastic scintillator bars of trapezoidal cross section, all with their long sides parallel to the beam direction. This geometry is similar to that of the CTOF [9].

As previously stated, one of the two requirements of the CND is good neutron identification capabilities. If the charged particles are vetoed by the central tracker, the only particles remaining from the target that can be misidentified for neutrons are photons. Using plastic scintillators, the most straightforward way to distinguish neutrons from photons is by measuring their time-of-flight (TOF) and comparing the values of  $\beta$ :

$$\beta = \frac{l}{TOF \cdot c}, \quad (1)$$

where  $c$  is the speed of light and  $l$  is flight path of the particle from the target to the scintillator bar. This can be obtained, in our geometry, as

$$l = \sqrt{z^2 + h^2}, \quad (2)$$

where  $z$  and  $h$  are the hit position along the beam  $z$  axis and in the radial direction, respectively. To obtain  $z$  one must measure the time of the hit at both ends of the scintillator bar:

$$z = \frac{1}{2} \cdot v_{eff} \cdot (t_{left} - t_{right}), \quad (3)$$

where  $v_{eff}$  is the effective velocity of light propagation in the scintillator material. To know  $h$  it is necessary to have reasonably small radial segmentation:  $h$  will be given by the distance between the target and the middle of the hit paddle.

GEANT4-based simulations show that to ensure a good photon/neutron separation for the neutron momentum range of the  $n$ -DVCS reaction the CND has to be

equipped with photodetectors ensuring a time resolution of about 150 ps.

### 3. Design

The design of the Central Neutron Detector is a barrel, coaxial with the beamline, made of trapezoidal scintillator bars, read out via standard PMTs attached to long Acrylic light guides. In order to optimize the light collection by matching the scintillator surface and the PMT entrance window, the detector is divided into 48 azimuthal segments and 3 radial layers, for a total of 24 blocks<sup>1</sup>, 144 scintillator bars, 144 PMTs, and 72 U-turn light guides (see Fig. 1). The radial thickness of all scintillators is 30 mm. The other dimensions are listed in Table 1.

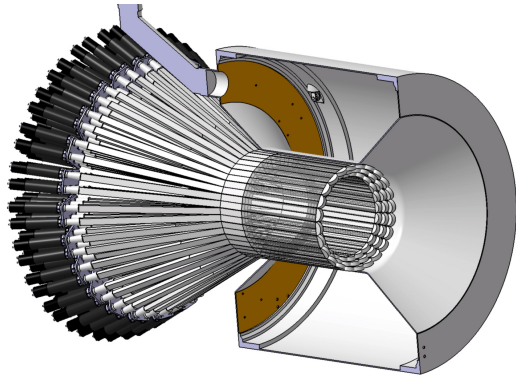


Figure 1: Drawing of the Central Neutron Detector inserted in the CLAS12 solenoid. A BETTER FIGURE IS NEEDED.

Layer	Inner face width (mm)	Outer face width (mm)	Length (mm)
1	35.92	39.87	665.72
2	40.0	43.95	700.0
3	44.08	48.03	734.28

Table 1: Dimensions (mm) of the trapezoidal scintillator bars of the CND. The layer numbers go from the innermost (1) to the outermost (3). The thickness of all bars is 30 mm.

### 4. Hardware Components and Construction

Comparative measurements were carried out to choose the elements composing the CND. The tests

<sup>1</sup>A “block” or “sector” is formed by three radial layers of coupled pairs of scintillator bars.

were geared towards optimizing the time resolution, which is the key parameter to ensure  $n/\gamma$  separation, and containing all associated costs. Different prototypes were constructed and employed for measurements of time resolution and light-yield during cosmic ray testing to optimize the final design choices for scintillator type, PMT, wrapping material, PMT magnetic shielding configuration, shape of the U-turn light guide, and glue for the optical coupling. The outcomes of these tests are discussed in detail in [8]. The chosen components are:

- 144 EJ200 scintillator bars, by Eljen Technology;
- 144 Hamamatsu R10533 2-in PMTs;
- 72 semi-circular-shaped U-turn light guides of Polymethyl Methacrylate (PMMA);
- aluminum foil as reflector material wrapping the scintillator bars;
- a 1-mm-thick mu-metal cylinder plus a 5-mm-thick mild steel cylinder to shield each PMT from the stray magnetic field of the CLAS12 solenoid;
- coupling with optical grease between PMT and light guide;
- M-Bond200 glue for the junctions between scintillators and light guides.

The 24 blocks composing the Central Neutron Detector were assembled in the mechanical shop of IPN Orsay [8] and then shipped to Jefferson Lab (JLab), along with the components of the support structure. The support structure consists of six separate aluminum arches that are fastened together to form a ring, which is in turn attached to the solenoid by means of stainless-steel brackets. The support structure was installed first onto the CLAS12 solenoid, and then the 24 blocks of the CND were inserted, one by one, and secured onto the structure. The PMTs, within their shieldings, were then connected to the end of the light guides, to which they were coupled with optical grease. Figure 2 shows the detector after its installation.

## 5. Electronics and readout

The completely resistive high-voltage dividers of the CND were designed following the voltage distribution ratio suggested by Hamamatsu. The tube-base assembly was developed at IPN Orsay with the aim to mechanically match the mild-steel PMT shielding, for a compact and robust design. In order to operate the PMTs, high



Figure 2: The Central Neutron Detector as installed in the CLAS12 solenoid.

voltages (typically in the range of 1500 V) are provided by multi-channel CAEN SY527 power supplies. The HV boards adopted for the CND are CAEN A734N (16 channels, 3 kV max voltage, 3 mA max current). The signal of each PMT is sent to an active splitter. The three splitter modules used for the CND were originally developed by IPN Orsay for the G0 experiment (Hall C, JLab) [10]. Each module is an active 64-channel splitter with unity gain, so that there is no loss of amplitude. The 64 SMA inputs are placed in the back panel. In the front panel there are 8 8-channel output connectors (DMCH) for the time signals and 4 16-channel output connectors (FASTBUS) for the charge signals. The charge signal from the splitter is sent to JLab-designed 16-channel 250 MHz VXS-based flash-ADCs. The time signal from the splitter is sent to a constant fraction discriminator (CFD) GANELEC FCC8, originally developed for the TAPS detector in Mainz. Each CFD module is an 8-channel CAMAC unit with LEMO 00 input connectors and 2x8-pin output connectors in differential ECL. The threshold can be set for each channel individually using a manual switch or remote control, and no time-walk adjustment is required for the module. The discriminated time signal then goes to the TDC (CAEN VX1290A, 32 channels/board, 25 ps/channel resolution). In total, the read-out system includes 3

Constant name	Number of constants	Units
$t_{LR}$	72	ns
$v_{eff}$	144	cm/ns
$u_t$	72	ns
$t_{LR_{ad}}$	72	ns
$t_{off}$	72	ns
$A_L$	144	cm
$MIP_D, MIP_T$	144 each	no units

Table 2: The constants computed in the CND calibration.

splitter modules, 19 CFD modules, 5 TDC boards, and 8 ADC boards.

## 6. Calibration

The calibration of the CND with beam data is done in two steps: the timing calibration, which allows us to obtain effective velocities and time offsets, which are, in turn, necessary to deduce timing and position information of the hits; and the energy calibration, in which attenuation lengths and energy conversion factors are extracted. Table 2 summarizes the calibration constants necessary to reconstruct CND hits.

### 6.1. Timing calibration

There are four calibration constants that must be determined as part of the CND timing calibration: the Left-Right time offset ( $t_{LR}$  and  $t_{LR_{ad}}$ ), the effective velocity ( $v_{eff}$ ), the propagation time in the U-turn ( $u_t$ ), and the global time offset with respect to the event start time ( $t_{off}$ ). The calibrations of these constants must be done in the following order:  $t_{LR}$ ,  $v_{eff}$ ,  $u_t$ ,  $t_{LR_{ad}}$ , and finally  $t_{off}$ . Each of these constants is determined using charged particles from beam interactions in the target.

The raw hit times  $t_{L/R}$  are obtained from the measured TDC channel using a slope constant of 0.0234 ns/channel for all channels.

The paddle in which the hit occurs must be determined before the calibration procedure can be applied. The left and right times of a hit in the left paddle (we label them as  $t_{L/L}$  and  $t_{R/L}$  where the first index corresponds to the paddle under exam, while the second indicates the paddle in which the primary hit happened) are given by:

$$t_{L/L} = t_{off} + t_{tof} + \frac{z}{v_{eff_L}} + t_S + t_{off_L} + TDC_j, \quad (4)$$

$$t_{R/L} = t_{off} + t_{tof} - \frac{z}{v_{eff_L}} + \frac{L}{v_{eff_L}} + \frac{L}{v_{eff_R}} + u_t + t_S + t_{off_R} + TDC_j. \quad (5)$$

where  $t_{tof}$  is the time of flight extracted using the CVT [11] path length information,  $z$  is the position of the hit measured from the upstream end of the paddle,  $L$  is the length of the paddle,  $t_S$  is the start time of the event,  $t_{off_L}$  and  $t_{off_R}$  are time offsets associated to the left and right coupled paddles, and  $TDC_j$  is the TDC clock jitter. Similarly if the hit happened in the right paddle one can write:

$$t_{L/R} = t_{off} + t_{tof} - \frac{z}{v_{eff_R}} + \frac{L}{v_{eff_L}} + \frac{L}{v_{eff_R}} + u_t + t_S + t_{off_L} + TDC_j, \quad (6)$$

$$t_{R/R} = t_{off} + t_{tof} + \frac{z}{v_{eff_R}} + t_S + t_{off_R} + TDC_j. \quad (7)$$

Defining  $\Delta$  and  $\Delta'$  as:

$$\Delta = \frac{L}{v_{eff_L}} - \frac{L}{v_{eff_R}}, \quad (8)$$

$$\Delta' = t_{L/X} - t_{R/X} + t_{off_R} - t_{off_L}, \quad (9)$$

where the index X can be R or L, one can compute  $\Delta - \Delta'$  for both cases (hit in the left paddle or hit in the right paddle). If the hit is in the left paddle:

$$\Delta' - \Delta = \frac{2z}{v_{eff_L}} - \frac{2L}{v_{eff_L}} - u_t < 0. \quad (10)$$

If the hit is in the right paddle:

$$\Delta' - \Delta = \frac{2L}{v_{eff_R}} - \frac{2z}{v_{eff_R}} + u_t > 0. \quad (11)$$

If  $\Delta' < \Delta$ , the paddle in which the hit happened is the left one, otherwise it is the right one. This procedure to determine the hit paddle depends on constants yet to be calibrated ( $v_{eff}$  and  $t_{off_R} - t_{off_L}$ ). Therefore, at least two iterations of the calibrations of  $v_{eff}$  and  $t_{off_R} - t_{off_L}$  are required.

#### 6.1.1. Left-right timing offset

The Left-Right time offset refers to the time misalignment between two coupled paddles. It is determined in two steps. The first step relies on the U-turn structure of the CND to extract an estimate of this offset  $t_{LR}$ . The second step corrects this first value to obtain the real value  $t_{LR_{ad}}$  by taking into account the effective velocities of both coupled paddles. There is one value of  $t_{LR}$  and  $t_{LR_{ad}}$  for each pair of paddles.

There are two different algorithms to find  $t_{LR}$  depending if the data were taken with our without magnetic field of the solenoid.

265

- If the solenoid field is off, the U-turn light guide coupling two adjacent CND paddles induces a gap in the time difference  $t_R - t_L$  plots. The  $t_{LR}$  constant is defined as the time difference value at the center of the gap.
- If the solenoid is on, “double hits” occur. When the trajectory of a charged particle bent in the solenoid field crosses two adjacent coupled paddles, the two L/R signals have very similar TDCs (see Fig. 3). Such hits induce a peak instead of a gap in the time difference plots (see Figure 4).  $t_{LR}$  is defined as the position of this peak.

270

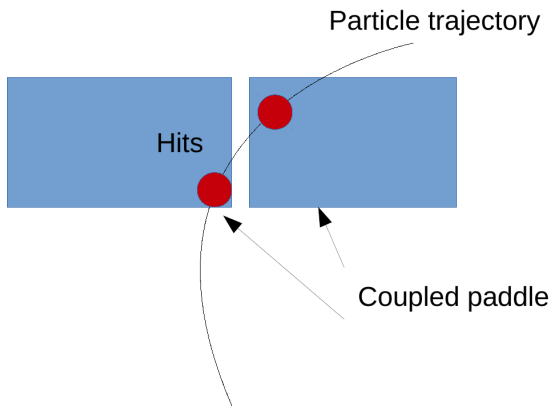


Figure 3: Double hits in the CND produced by the curved trajectory of a charged particle in the solenoid field. Both hits have similar TDCs resulting in a peak in the time difference distribution.

275

Both cases are illustrated in Fig. 4. Typical values for the offsets are below 5 ns.  $t_{LR}$  is not used in the reconstruction, but it is nonetheless necessary to remove double hits from the subsequent calibration steps.  $t_{LR_{ad}}$ , defined below, is used in the reconstruction. Once  $t_{LR}$  constants has been determined, they are corrected to account for the different effective velocities of the two coupled paddles.

280

For hits in the left paddle, the two associated TDCs can be expressed as:

$$t_L = t_{\text{off}} + t_{\text{tof}} + \frac{z}{v_{\text{eff}_L}} + t_S + t_{\text{off}_L} + \text{TDC}_j, \quad (12)$$

$$t_R = t_{\text{off}} + t_{\text{tof}} - \frac{z}{v_{\text{eff}_L}} + \frac{L}{v_{\text{eff}_L}} + \frac{L}{v_{\text{eff}_R}} + u_t + t_S + t_{\text{off}_R} + \text{TDC}_j. \quad (13)$$

285

$t_{LR_{ad}}$  is defined as:

$$t_{LR_{ad}} = t_{\text{off}_R} - t_{\text{off}_L}. \quad (14) \quad 295$$

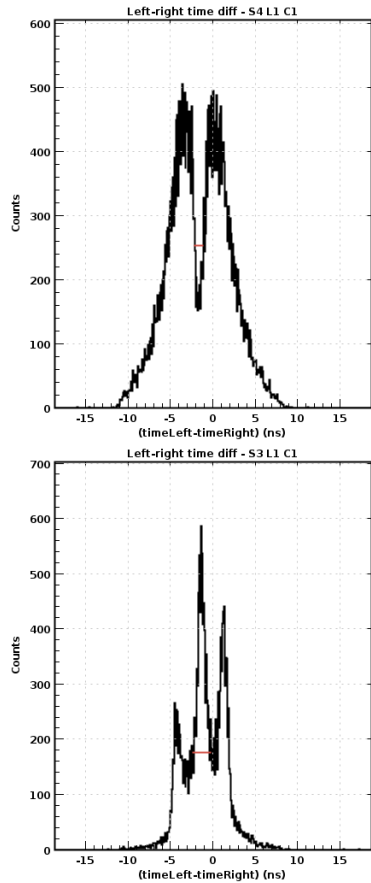


Figure 4: Left-right time difference. The top plot is for zero solenoid field: the U-turn light guide induces a gap in the distribution. The bottom plot is for data with magnetic field: double hits, with equal TDCs, produce a peak instead of a gap.

Then one can write:

$$\frac{t_{L-t_R}}{2} = \frac{z}{v_{\text{eff}_L}} - \frac{L}{2 \cdot v_{\text{eff}_L}} - \frac{L}{2 \cdot v_{\text{eff}_R}} - \frac{u_t}{2} - \frac{t_{LR_{ad}}}{2}. \quad (15)$$

The negative of the intercept of  $\frac{t_{L-t_R}}{2}$  vs.  $z$  is equal to:

$$C_L = \frac{L}{2 \cdot v_{\text{eff}_L}} + \frac{L}{2 \cdot v_{\text{eff}_R}} + \frac{u_t}{2} + \frac{t_{LR_{ad}}}{2}. \quad (16)$$

For hits in the right paddle, the corresponding equation reads:

$$C_R = \frac{L}{2 \cdot v_{\text{eff}_R}} + \frac{L}{2 \cdot v_{\text{eff}_L}} + \frac{u_t}{2} - \frac{t_{LR_{ad}}}{2}. \quad (17)$$

Combining equations 16 and 17,  $t_{LR_{ad}}$  is given by:

$$t_{LR_{ad}} = C_L - C_R. \quad (18)$$

### 6.1.2. Effective velocity

The effective velocity  $v_{\text{eff}}$  is the speed of the light in the scintillators and the light guides. There is one  $v_{\text{eff}}$  value for each paddle.  $v_{\text{eff}}$  is obtained from the following equation:

$$z = (t_L - t_R) \cdot \frac{v_{\text{eff}}}{2} + c, \quad (19)$$

where  $z$  is the  $z$  position of the hit in the CND with respect to the upstream end of the CND paddles and  $c$  is an unknown constant.  $z$  is obtained independently from the CND, using the CVT. The above equation is true for hits in left paddles. For hits in the right paddles, the sign of the time difference must be changed.  $v_{\text{eff}}$  is extracted by fitting the  $\frac{t_R - t_L}{2}$  vs.  $z$  distribution as shown in Fig. 5. For each slice in  $z$ , the position of the maximum from a Gaussian fit is plotted against  $z$ . The gradient of the obtained distribution gives  $v_{\text{eff}}$ . The expected values for  $v_{\text{eff}}$  are around 16 cm/ns.

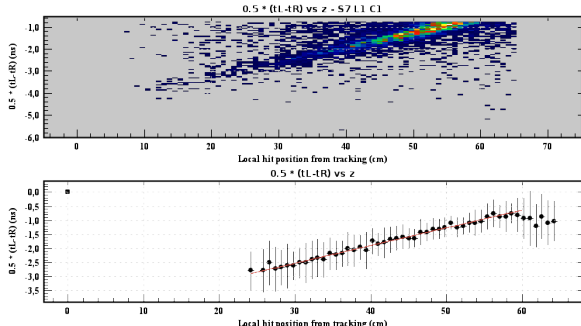


Figure 5: Plots used to determine the effective velocity for a CND paddle. The two plot is the raw  $\frac{t_R - t_L}{2}$  vs  $z$  and the bottom plot is the distribution showing the linear fit.

### 6.1.3. U-turn propagation time

The U-turn propagation time  $u_t$  is the time spent by the light to travel through the U-turn light guide. It is used as a time offset on the indirect signal in the time and position reconstruction. There is one  $u_t$  value for each pair of paddles. The algorithm to extract  $u_t$  is very similar to the one used in the  $v_{\text{eff}}$  procedure: the intercept of the  $\frac{t_R - t_L}{2}$  vs.  $z$  (see Fig. 5) is extracted for both coupled paddles to determine  $u_t$ .

Recalling Eq. 12, the half time difference can be written :

$$\frac{t_L - t_R}{2} = \frac{z}{v_{\text{eff}_L}} - \frac{L}{2 \cdot v_{\text{eff}_L}} - \frac{L}{2 \cdot v_{\text{eff}_R}} - \frac{u_t}{2} - \frac{t_{LR_{\text{ad}}}}{2}, \quad (20)$$

thus the negative of the intercept of the linear fit of  $\frac{t_L - t_R}{2}$  vs.  $z$  is equal to:

$$C_L = \frac{L}{2 \cdot v_{\text{eff}_L}} + \frac{L}{2 \cdot v_{\text{eff}_R}} + \frac{u_t}{2} + \frac{t_{LR_{\text{ad}}}}{2}. \quad (21)$$

For hits in the right paddle:

$$C_R = \frac{L}{2 \cdot v_{\text{eff}_R}} + \frac{L}{2 \cdot v_{\text{eff}_L}} + \frac{u_t}{2} - \frac{t_{LR_{\text{ad}}}}{2}. \quad (22)$$

Combining Eqs. 21 and 22,  $u_t$  is given by :

$$u_t = C_R + C_L - L \left( \frac{1}{v_{\text{eff}_R}} + \frac{1}{v_{\text{eff}_L}} \right). \quad (23)$$

The values for  $u_t$  are typically in the 0.5 ns - 1.5 ns range, with layer 1 values around 0.6 ns, layer 2 around 1 ns, and layer 3 around 1.4 ns.

### 6.1.4. Global time offset

The global time offset  $t_{\text{off}}$  refers to the time difference between the start time value and the vertex time computed from the CND hit time and the CVT path length information. There is one  $t_{\text{off}}$  value for each pair of coupled paddles.  $t_{\text{off}}$  is given by the following equation :

$$t_{\text{off}} = \frac{t_L + t_R}{2} - t_S - t_{\text{tof}} - \frac{L}{2} \cdot \left( \frac{1}{v_{\text{eff}_R}} + \frac{1}{v_{\text{eff}_L}} \right) - \frac{u_t}{2} - \frac{t_{LR_{\text{ad}}}}{2} - \text{TDC}_j, \quad (24)$$

where  $t_{\text{tof}}$  is calculated using CVT information assuming the particles are pions. For this, a negative charge is required, as most of the negative particles in the Central Detector are pions. The position of the peak of the above distribution gives  $t_{\text{off}}$ . Its values depend mainly on the start time values, which is calculated using the CLAS12 FTOF system [12]. The variations of  $t_{\text{off}}$  between different pairs of paddles are typically below 10 ns.

## 6.2. Energy calibration

There are three calibration constants for the energy determination in each paddle of the CND: the attenuation length ( $A_L$ ), the ADC-to-energy constants for direct minimum-ionizing particles (MIPs) ( $MIP_D$ ), and the ADC-to-energy constants for indirect MIP ( $MIP_I$ ). These three calibration steps can be performed almost independently from the timing calibration, however,  $t_{LR_{\text{ad}}}$  is needed to determine if an ADC signal is direct or indirect (ie the hit happened in the considered paddle or in its coupled partner).

### 6.2.1. Attenuation length

The attenuation length  $A_L$  accounts for the light attenuation along the length of the scintillators and light guides. There is an  $A_L$  value for each paddle. For hits in the left paddle, the two associated ADCs can be written as:

$$ADC_L = \frac{E}{E_0} \cdot MIP_D \cdot e^{-\frac{z}{A_L}}, \quad (25)$$

$$ADC_R = \frac{E}{E_0} \cdot MIP_I \cdot e^{-\frac{(L-z)}{A_L}}, \quad (26)$$

where  $MIP_D$  and  $MIP_I$  are constants defined in the Section 6.2.2,  $E$  is half the energy deposited by the particle in the scintillator, and  $E_0$  is half the energy deposited by a MIP in the scintillators.  $E_0$  is given by:

$$E_0 = \frac{h \cdot 1.956}{2} \text{ MeV}, \quad (27)$$

where  $h$  is the thickness of each scintillator. All the above equations are valid for hits in the left paddles, while for hits in the right paddles the corresponding equations are obtained by switching the indices. From Eqs. 25 and 26 the following relation is derived:

$$\ln(ADC_L/ADC_R) = c - \frac{2 \cdot z}{A_L}, \quad (28)$$

where  $c$  is a constant depending on  $MIP_D$ ,  $MIP_I$ , and  $L$ .  $A_L$  is given by the slope of the distribution in Eq. 28 as shown in Fig. 6. Values for  $A_L$  are typically around 150 cm.

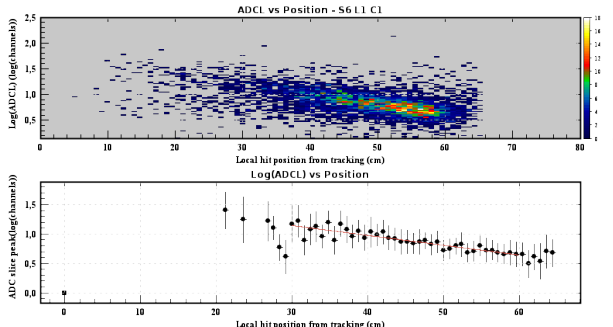


Figure 6: Plots used to determine  $A_L$ . The left plots corresponds to the left paddle and the right ones to the right paddle. The top two plots show the raw  $\ln(ADC_L/ADC_R)$  vs.  $z$  distributions. Slices in  $z$  are fitted with a Gaussian and the mean is plotted against  $z$ . The corresponding distributions and their associated linear fits are shown in the bottom two plots.

### 6.2.2. Energy calibration

The final step of the calibration of the CND is the determination of the energy conversion parameters  $MIP_D$  and  $MIP_I$ . There are two energy parameters for each paddle, thus there are four energy parameters for each pair of coupled paddles, denoted as  $MIP_{DL}$ ,  $MIP_{IL}$ ,  $MIP_{DR}$ ,  $MIP_{IR}$ .

In the following, we only consider a hit in the left paddle. Equations for hits in right paddles are obtained by switching the indices. For hits in the left paddle, only  $MIP_{DL}$  and  $MIP_{IL}$  can be obtained. In the following they are referred to as  $MIP_D$  and  $MIP_I$ . From Eqs. 25 and 26, one gets:

$$\ln\left(\frac{ADC_L}{ADC_R}\right) = \ln\left(\frac{MIP_D}{MIP_I}\right) + \frac{L}{A_L} - \frac{2 \cdot z}{A_L} \quad (29)$$

$$\sqrt{ADC_L \cdot ADC_R} = \frac{E}{E_0} \cdot \sqrt{MIP_D \cdot MIP_I} e^{-\frac{L}{2A_L}}. \quad (30)$$

From Eq. 29, the intercept of the  $\ln\left(\frac{ADC_L}{ADC_R}\right)$  vs.  $z$  distribution gives the ratio  $\frac{MIP_D}{MIP_I}$ . The same distributions as in Fig. 5 are used to extract the intercept. The product  $MIP_D \cdot MIP_I$  is obtained using Eq. 30 after filtering MIPs and correcting for the path travelled by the MIP in the scintillators. Indeed for MIPs,  $E$  can be written as:

$$E = \frac{\text{path}}{h} \cdot E_0, \quad (31)$$

where  $\text{path}$  is the path travelled by the MIP in the scintillator, which is obtained using the CVT tracking information by extrapolating the particle trajectory at the radius of the CND hit. Selecting MIPs and correcting for the path length removes the energy dependence from Eq. 30, which becomes:

$$\sqrt{ADC_L \cdot ADC_R} = \frac{\text{path}}{h} \cdot \sqrt{MIP_D \cdot MIP_I} e^{-\frac{L}{2A_L}}. \quad (32)$$

The distribution of  $\sqrt{ADC_L \cdot ADC_R} \cdot \frac{h}{\text{path}}$  is fitted with a Landau function and the position of the peak  $p$  is extracted as shown in Fig. 7.  $MIP_D$  and  $MIP_I$  are given by:

$$MIP_D = \sqrt{e^{i-\frac{L}{A_L}} \cdot e^{\frac{L}{A_L}} \cdot p^2}, \quad (33)$$

$$MIP_I = \sqrt{e^{-\left(i-\frac{L}{A_L}\right)} \cdot e^{\frac{L}{A_L}} \cdot p^2}, \quad (34)$$

where  $i$  and  $p$  are the intercept and peak position defined above.  $MIP_D$  and  $MIP_I$  are typically around 2000 and 500, respectively.

In the following sections the reconstruction algorithms are described.

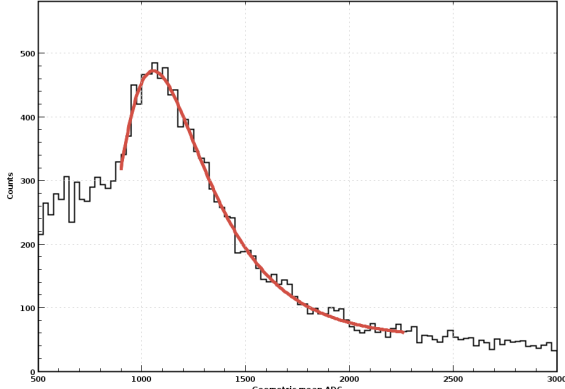


Figure 7:  $\sqrt{ADC_L \cdot ADC_R} \cdot \frac{h}{path}$  distribution fitted with a Landau function. The events in this plot are identified as MIPs by requiring a pion. The PID is performed asking for negative charge, as most negatively charged particles in the Central Detector are pions.

## 7. Reconstruction

The reconstruction of the CND is done in three steps:

- the reconstruction of the deposited energy;
- the reconstruction of the time and position of the hit in the paddle;
- the matching of CND hits with tracks coming from the interaction vertex.

### 7.1. Energy reconstruction

For hits in the left paddle, the two associated ADCs can be written as:

$$ADC_L = \frac{E_L}{E_0} \cdot MIP_D \cdot e^{\frac{-z}{A_L}}, \quad (35)$$

$$ADC_R = \frac{E_R}{E_0} \cdot MIP_I \cdot e^{\frac{-(L-z)}{A_L}}, \quad (36)$$

where  $E_{L/R}$  is half the energy deposited by the particle in the left/right paddle and  $E_0$  is given by Eq. 27. The above equations are valid for hits in the left paddles, while for hits in the right paddles, the applicable equations are obtained by switching the  $L/R$  indices. From Eqs. 35 and 36 follows the relations:

$$E_L = \frac{ADC_L \cdot E_0}{MIP_D} \cdot e^{\frac{z}{A_L}}, \quad (37)$$

$$E_R = \frac{ADC_R \cdot E_0}{MIP_I} \cdot e^{\frac{L-z}{A_L}}. \quad (38)$$

The total deposited energy is given by the sum of  $E_L$  and  $E_R$ :

$$E_{\text{dep}} = E_L + E_R. \quad (39)$$

### 7.2. Hit position and time reconstruction

The reconstruction of the time and position of a hit will be shown for the case of a hit in the left paddle. In case of a hit in the right paddle the applicable equations are obtained by switching the  $L/R$  indices.

Starting from  $t_L$  and  $t_R$ , defined in Eq. 6 and subtracting the time offsets obtained from the calibrations, the start time and the time jitter, one can define the propagation times  $t_{L,\text{prop}}$  and  $t_{R,\text{prop}}$  as:

$$t_{L,\text{prop}} = t_{\text{tof}} + \frac{z}{v_{\text{eff},L}}, \quad (40)$$

$$t_{R,\text{prop}} = t_{\text{tof}} - \frac{z}{v_{\text{eff},L}} + \frac{L}{v_{\text{eff},L}} + \frac{L}{v_{\text{eff},R}} + u_t. \quad (41)$$

The position of the hit is then obtained as the difference of the propagation times:

$$z = \frac{v_{\text{eff},L}}{2} \left( t_{L,\text{prop}} - t_{R,\text{prop}} + L \cdot \left( \frac{1}{v_{\text{eff},L}} + \frac{1}{v_{\text{eff},R}} \right) + u_t \right). \quad (42)$$

The  $x$  and  $y$  coordinates of the hit are obtained from the radius and the azimuthal angle of the hit, which are, in turn, determined by knowing the layer, sector, and component (left or right) of the hit. Finally, the time of flight of the particle that produced the hit is obtained as:

$$t_{\text{tof}} = \frac{1}{2} \left( t_{L,\text{prop}} + t_{R,\text{prop}} - L \cdot \left( \frac{1}{v_{\text{eff},L}} + \frac{1}{v_{\text{eff},R}} \right) - u_t \right). \quad (43)$$

### 7.3. Hit/Track matching

Tracks from charged particles crossing the CVT are associated to hits in the CND. This allows, for each CND hit matched with a CVT track, to calculate the position of the hit from the extrapolated track, the path-length between the track vertex and the hit and the path travelled in the hit paddle. This information is used in the calibration (Section 6), as well as to veto charged particles when looking for neutrons in the CND. CVT tracks are extrapolated to radii corresponding to the entry point, middle point and exit point of the track in the paddle. These points are defined as the intersections between the helix of the track and cylinders of radii corresponding to the distances between the center of the CD and the three CND layers. A CVT track and a CND hit are matched if the hit coordinates ( $x$ ,  $y$ , and  $z$ ) and the extrapolated coordinates ( $x_m$ ,  $y_m$ , and  $z_m$ ) verify the relations:

$$|x - x_m| < \sigma_x, \quad (44)$$

$$|y - y_m| < \sigma_y, \quad (45)$$

$$z_m \in [-\sigma_z, L + \sigma_z], \quad (46)$$

490 where  $\sigma_z = 1.5$  cm,  $L$  is the length of a paddle, and  $\sigma_x$  and  $\sigma_y$  are given by:

$$\sigma_x = \sqrt{x^2 \frac{\sigma_R^2}{R^2} + y^2 \sigma_\phi^2}, \quad (47)$$

$$\sigma_y = \sqrt{y^2 \frac{\sigma_R^2}{R^2} + x^2 \sigma_\phi^2}, \quad (48)$$

495 where  $R$  is the radius of the hit,  $\sigma_R$  is half the thickness  
of a paddle (1.5 cm) and  $\sigma_\phi$  is the azimuthal resolution  
of each paddle (3.75). The path travelled by the particle  
in the paddle is approximated as the distance between  
the entry and exit points.

500 The path length between the vertex and the hit is  
given by the helix parameters. (this last part needs to  
be developed)

## 8. Simulation

505 In order to study the performance of the CND, its  
geometry and response were included in the CLAS12  
GEANT4-based simulation package, GEMC. The Birks  
effect, for which the amount of optical photons pro-  
duced after a certain energy deposition in the scintilla-  
510 tor depends on the particle losing that energy, and the  
hit digitization for the CND have been introduced in  
GEMC. The timing resolution and the energy loss due to  
the U-turn geometry were included in the simulation us-  
ing the values measured in the cosmic-ray tests. Details  
515 on the digitization and on the hit and event reconstruc-  
tion are explained in [13] and 7), respectively.

520 Simulations were run to evaluate the efficiency of the  
CND for neutrons, its ability to discriminate between  
neutrons and photons, and its angular and momentum  
resolutions. Neutrons and photons of momenta vary-  
ing between 0.1 and 1 GeV and having polar angles  $\theta$   
525 between  $50^\circ$  and  $70^\circ$  were generated at fixed azimuthal  
angle ( $\phi = 3.75^\circ$ ). Several values of energy thresholds,  
between 1 and 5 MeV, were studied. Figure 8 shows the  
neutron detection efficiency, which decreases with in-  
creasing threshold and ranges between 12% at the low-  
530 est thresholds and 7% at the highest ones. The angular  
resolution  $\sigma_\theta$ , obtained via Gaussian fits of the simu-  
lated  $\theta$  distributions, increases slightly with the angle  
and also is fairly constant as a function of neutron momen-  
tum with its values between  $1.8^\circ$  and  $3^\circ$ . The res-  
535 olution on the azimuthal angle is directly connected to  
the total number of scintillator bars along  $\phi$ . The an-  
gular size of each bar,  $\Delta\phi$ , being  $7.5^\circ$ ,  $\sigma_\phi$  is given by

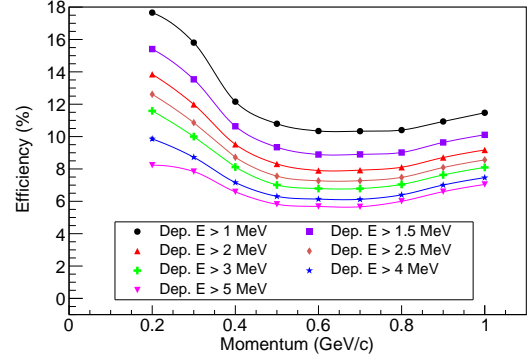


Figure 8: Simulation results for the efficiency for the detection of neutrons emitted at  $60^\circ$  as a function of momentum for 7 different values of the threshold on the deposited energy, from 1 to 5 MeV.

535  $\Delta\phi/2 = 3.75^\circ$ . The resolution on the neutron momentum, which is obtained knowing  $\beta$  and having performed the particle identification, according to the formula

$$p = \frac{\beta \cdot m_n}{\sqrt{1 - \beta^2}}, \quad (49)$$

is also strictly connected to the time resolution. The momentum resolution  $\sigma_p/p$  ranges between 4.5% and 6%, for increasing neutron momentum. No appreciable variation of momentum resolution was observed by varying the neutron polar angle. As for the  $\theta$  reconstruction, also in this case the reconstructed momentum was computed as the average over all layers, whenever more than one layer had a good hit.

540 Since the charged particles passing through the CND will be vetoed by the Central Tracker, the only particles that could be mistaken for neutrons in the CND are the photons. The efficiency of the CND for photons has been estimated by simulations, and it is slightly larger than the one for neutrons (of the order of 15%, having little energy dependence). Neutrons can be discriminated from photons by means of their  $\beta$ . Therefore, the  $\beta$  distributions that can be obtained with the CND for neutrons and photons were studied with the help of the GEMC simulation. After choosing a good hit,  $\beta$  is computed as

$$545 \beta = \frac{l}{TOF_{true} \cdot c}, \quad (50)$$

550 where

$$l = \sqrt{h^2 + z_{ave}^2}. \quad (51)$$

555  $h$  is the distance from the vertex to the middle of the layer where the hit took place,  $TOF_{true}$  is the recon-

structed time-of-flight and  $z_{ave}$  is the reconstructed position of the hit along the scintillator bar. Figure 9 shows the comparison between the  $\beta$  distributions obtained for neutrons of various momenta (0.2, 0.4, 0.7 and 1 GeV) and for 1-GeV photons. All particles in this plot were emitted at  $\theta = 60^\circ$ . A small portion of the neutrons having momentum of 1 GeV can be taken as photons, as their  $\beta$  distributions begin to overlap, while the  $n/\gamma$  separation is clear for lower momenta — which corresponds to most of the range of interest for  $n$ -DVCS, as only about 8% of the events are expected to have  $p_n > 0.9$  GeV.

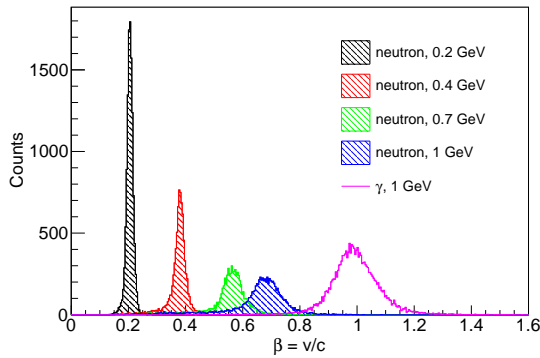


Figure 9: Simulation results for the  $\beta$  distributions for neutrons with  $p_n = 0.2$  GeV (black),  $p_n = 0.4$  GeV (red),  $p_n = 0.7$  GeV (green),  $p_n = 1$  GeV (blue), and photons with  $E = 1$  GeV (purple). The threshold on the deposited energy is 3 MeV. The plot show all reconstructed particles integrated over  $\phi$ . Equal neutron and photon yields were assumed.

570

### 8.1. CND-based veto of charged particles

Section to be developed.

## 9. Performance

Data taken during the first CLAS12 experiments, on hydrogen and deuterium targets, and with various beam energies (6.6 and 10.6 GeV), were analyzed to verify the performances of the CND. 575 600

The timing performances for the three layers of the CND are illustrated in Fig. 10, that shows the vertex time difference  $v_t$  for selected negative tracks, integrated over all sectors. It is defined as 580 605

$$v_t = t_{\text{CND}} - t_S - \frac{\text{path}}{c \cdot \beta} \quad (52)$$

where  $t_S$  is the event start time determined by the FTOF, 610  $\text{path}$  is the distance, computed by the CVT, travelled by

the particle from the target to the CND impact point, and

$$\beta = \frac{p}{\sqrt{p^2 + m^2}}. \quad (53)$$

The distribution of  $v_t$  is centered at 0, and from its width, obtained with a Gaussian fit ( $\sigma_{v_t} \simeq 243$  ps in average) one can deduce the average timing resolution for each PMT of the CND, convoluted with the CVT resolution, using the formula:

$$\sigma_t = \frac{\sqrt{\sigma_{v_t}^2 - \sigma_{t_S}^2}}{\sqrt{2}} = 157 \text{ ps}, \quad (54)$$

assuming  $\sigma_{t_S} = 80$  ps [12]. This is compatible with the detector specifications (150 ps) and the result of the measurements in cosmic rays during the detector assembly phase [8] (148 ps).

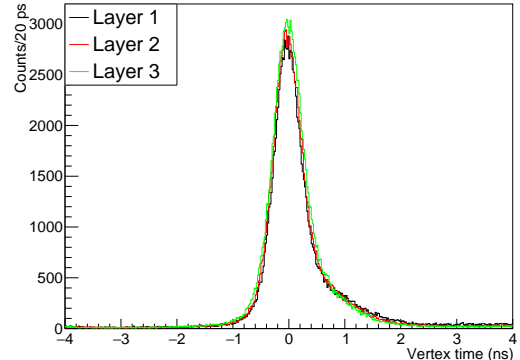


Figure 10: Difference between the vertex time computed combining CND and CVT information and the start time computed by the FTOF, for negative tracks, for the three layers of the CND, integrated over all paddles.

The position reconstruction performances of the CND can be checked in Fig. 12, which displays the difference between the  $z$  coordinate computed by the CND and by the CVT, for negative tracks, and for the three layers of the CND, integrated over all paddles. Its Gaussian width is around 3 cm, corresponding roughly to  $4^\circ$  in polar-angle resolution. This corresponds to the convolution of the angular resolutions of CND and CVT.

Figure 13 shows the energy deposit divided by path length, for selected MIPs. It peaks at around the expected value of 1.956 MeV/cm.

NEUTRON EFFICIENCY FIGURES ARE NOT READY YET, WE'RE WAITING FOR RGK DATA TO BE COOKED.

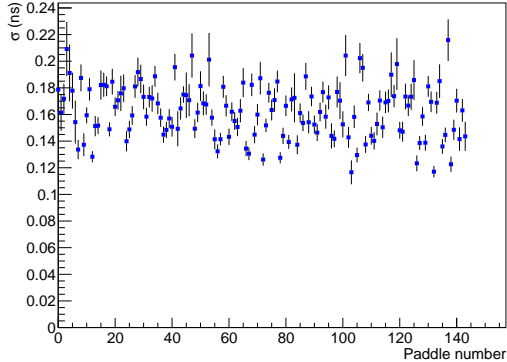


Figure 11: Timing resolution for each PMT of the CND, convoluted with CVT resolution.

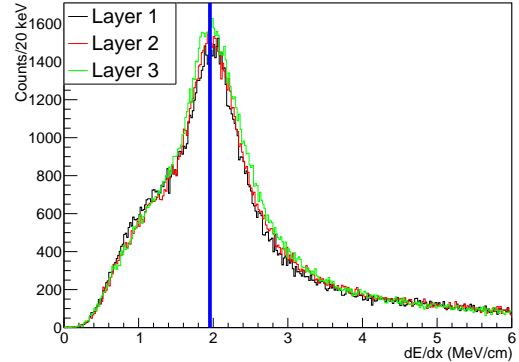


Figure 13:  $dE/dx$  for MIPs in the three layers of the CND, integrated over all sectors. The blue line indicates the nominal value for the expected energy deposit of a MIP in a centimeter of plastic scintillator.

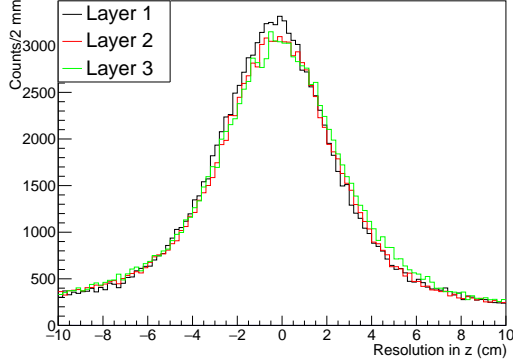


Figure 12: Difference between the  $z$  computed by the CND and the one provided by the CVT, for negative tracks, for the three layers of the CND, integrated over all paddles.

## 10. Acknowledgements

## 11. Conclusion

## 12. References

- [1] S. Niccolai, et al., Jefferson Lab experiment E12 – 11 – 003.
- [2] S. Niccolai, et al., Jefferson Lab experiment E12 – 06 – 109a.
- [3] D. Muller, D. Robaschik, B. Geyer, F. M. Dittes, J. Horejši, Wave functions, evolution equations and evolution kernels from light ray operators of QCD, *Fortsch. Phys.* 42 (1994) 101–141. [arXiv:hep-ph/9812448](https://arxiv.org/abs/hep-ph/9812448), doi:10.1002/prop.2190420202.
- [4] X.-D. Ji, Gauge-Invariant Decomposition of Nucleon Spin, *Phys. Rev. Lett.* 78 (1997) 610–613. [arXiv:hep-ph/9603249](https://arxiv.org/abs/hep-ph/9603249), doi:10.1103/PhysRevLett.78.610.
- [5] A. V. Radyushkin, Scaling limit of deeply virtual Compton scattering, *Phys. Lett.* B380 (1996) 417–425. [arXiv:hep-ph/9604317](https://arxiv.org/abs/hep-ph/9604317), doi:10.1016/0370-2693(96)00528-X.
- [6] , *Nucl. Instrum. Meth.*